Application of Fractional Integral Model in Construction of Image Enhancement Mask

Varsha S N [1,3,*] and Sowmya M [2,3]

[1] Department of Mathematics, Mount Carmel College, Autonomous, Bengaluru, India
[2] Department of Mathematics, RV College of Engineering, Bengaluru, India
[3] Faculty of Mathematics, Visvesvaraya Technological University, Belagavi, India
Email: varsha.sn@mccblr.edu.in (V.S.N.); sowmyam@rvce.edu.in (S.M.)
*Corresponding author

***Abstract*—Image enhancement is crucial in image processing applications to improve visual quality for better interpretation and analysis. Conventional enhancement techniques that rely on integer-order operators frequently have trouble striking a balance between feature retention and noise reduction. In this work, we propose a 5 × 5 and 7 × 7 fractional-order mask using the Caputo fractional integral, which offers a more flexible and accurate approach to image enhancement. To evaluate the effectiveness of the proposed approach, Gaussian noise is added to test images and the enhancement performance is quantitatively assessed using the Peak Signal-to-Noise Ratio (PSNR) and Structural Similarity Index Measure (SSIM). The experimental results demonstrate that the proposed fractional integral masks effectively enhance image quality by improving texture visibility and edge details while reducing noise. In particular, as the fractional order approaches one, the enhanced images show significant improvement in both PSNR and SSIM values, indicating better structural preservation and visual fidelity. These results confirm that the proposed Caputo fractional integral-based mask provides a flexible and effective alternative for image enhancement.**

***Keywords*—fractional calculus, image processing, image enhancement, fractional integral, Peak Signal-to-Noise Ratio (PSNR), fractional-order mask**

I. Introduction

Fractional calculus is a natural generalization of classical calculus, allowing integrals and derivatives of arbitrary (non-integer) order [1]. The concept of fractional operators emerged alongside classical operators, with the first known reference dating back to a 1695 correspondence between G. W. Leibniz and the Marquis de L'Hopital. Over time, prominent mathematicians like Euler, Liouville, and Laplace contributed to the development of this field, which has since become foundational in various practical domains such as fractional differential equations, fractional geometry, and fractional dynamics. Today, fractional calculus is widely applied across disciplines like rheology, acoustics, optics, control theory, and engineering, offering improved accuracy and flexibility compared to traditional integer-order models. Its ability to account for non-local and memory effects makes it especially useful for describing complex, real-world systems. In image processing, fractional calculus enhances tasks such as noise reduction, edge detection, and image enhancement by providing a more nuanced approach to capturing intricate image features.

An image is defined as a two-dimensional function, $F(x, y)$, where the amplitude of F at a specific coordinate (x, y) represents the image's intensity. When the values of F's x, y, and amplitude are finite, the image is considered a digital image. A digital image is essentially a two-dimensional array of components arranged in rows and columns, with each component having a distinct value at a given location, known as a pixel or picture element. Digital image processing refers to the use of a computer to process these digital images, often through algorithms, to enhance the image or extract relevant information.

Fractional calculus in image processing offers several advantages, including improved edge detection by capturing subtle image details, enhanced feature extraction through sensitivity to texture and structural variations, and better noise reduction while preserving important details. It can capture non-local information, making it more effective for complex images with intricate patterns. Additionally, fractional derivatives provide greater flexibility and more degrees of freedom than traditional integer-order methods, resulting in superior image enhancement and more accurate processing.

Image enhancement is the process of manipulating an image so that the result is more suitable than the original image for a specific application [2]. A key method in image processing technology, image enhancement aims to improve representation for computer vision algorithms and improve visual attractiveness. It tries to draw attention to the shortcomings of the existing picture enhancement methods and covers a variety of image kinds, such as color, grayscale, infrared, and films. Image processing is the process of improving an image's quality without sacrificing any information. Contrast enhancement is used

Manuscript received January 2, 2026; revised January 19, 2026; accepted April 14, 2026; published September 10, 2026.

in medical images to increase the brightness of the pixels. Image enhancement techniques require accurate input images that are appropriate for the particular algorithms used in computer vision.

II. Literature Review

The following literature demonstrates the significant potential of fractional calculus in enhancing various aspects of image processing, from edge detection to texture enhancement and noise reduction. The papers reviewed highlight various advancements in Fractional Calculus (FC) applications for image processing.

The application of fractional calculus in image processing has evolved significantly over the past few decades. Early theoretical foundations were established by Oldham and Spanier [1], who formalized the principles of fractional differentiation and integration. Traditional image processing techniques, relied on integer-order derivatives for edge detection and texture analysis but often struggled with noise sensitivity and loss of fine details [2, 3]. To address these limitations, Zhang *et al.* [4] introduced fractional differential masks based on the Riemann-Liouville (R-L) definition, demonstrating improved texture.

Subsequent works further refined these masks using Grünwald-Letnikov (G-L) approximations for enhanced edge detection [5, 6]. A texture improvement technique based on the Riesz fractional differential operator shows how well it can improve image texture features while maintaining crucial structural details [7]. A thorough analysis of several image-enhancing techniques also examines their methods, benefits, drawbacks, and applicability for diverse image kinds [8]. The introduction of non-singular kernel derivatives by Caputo and Fabrizio [9] marked a significant advancement, reducing numerical instability in fractional operators.

Using fractional-order calculus, Amoako-Yirenkyi *et al.* [10] shows enhanced edge analysis by introducing a novel picture edge detection mask built with the Riemann-Liouville fractional derivative. Amoako-Yirenkyi *et al.* [11] examines how well different picture smoothing methods work with a recently created fractional convolution mask, demonstrating how well it improves edge detection results. Applications in medical imaging, such as lung cancer segmentation [12] and radiographic edge detection [13], highlight the practical utility of fractional methods. The ideas, categories, and relative effectiveness of a variety of image enhancement approaches in enhancing image quality across a range of applications are reviewed [14].

Recent studies have leveraged the Caputo-Fabrizio (C-F) derivative for robust edge detection [15, 16], while some studies [17, 18] explored Atangana-Baleanu (A-B) derivatives for adaptive denoising. The latest developments continue to optimize fractional masks for real-time and domain-specific enhancements, underscoring the growing importance of fractional calculus in modern image processing [19, 20]. Fractional-order techniques for color image processing are examined in the study [21], which shows how fractional calculus can be used to edit and improve color photographs with higher visual quality. Nchama *et al.* [22] describes the creation of a Caputo fractional differential mask for picture enhancement, demonstrating that the proposed technique successfully enhances image quality by maintaining edges and highlighting fine details.

Fractional calculus has been widely adopted in image enhancement and denoising due to its ability to preserve texture and edge information while suppressing noise more effectively than integer-order methods. Al-Shamasneh and Ibrahim [23] introduced a local fractional entropy-based denoising model that enhances texture preservation and achieves improved PSNR performance. A fractional integral Retinex framework for image enhancement was proposed by Yu and Qin [24], showing that fractional operators reduce over-smoothing and retain fine structural details more effectively than Gaussian-based filters.

Nosheen *et al.* [25] investigated Caputo fractional derivatives and Caputo-Fabrizio integral operators, providing theoretical bounds that support the stability of fractional operators. Medved' *et al.* [26] developed nonlinear integral inequalities for tempered Ψ-Hilfer fractional integrals and analyzed fractional equations with tempered Ψ-Caputo derivatives, offering tools to model memory and attenuation effects in fractional-order systems. Huseynov *et al.* [27] derived generalized fractional Leibniz integral rules for Riemann-Liouville and Caputo derivatives, which are essential for the mathematical formulation and numerical implementation of Caputo-based fractional masks in image enhancement applications. Pu *et al.* [28] proposed a class of high-precision fractional differential masks derived from the Grünwald-Letnikov and Riemann-Liouville definitions, demonstrating that fractional-order operators can nonlinearly enhance texture details in smooth image regions more effectively than traditional integer-order differential methods.

The most common ways to improve fractional images are to, use Riemann-Liouville, Grünwald-Letnikov, and Riesz differential formulations to improve edges and textures [4, 6, 7, 10, 28]. More recently, these methods have been extended to include non-singular kernels like Caputo-Fabrizio and Atangana-Baleanu operators [9, 17, 22]. But these methods are mostly based on derivatives and focus on making edges more visible instead of getting a balance between smoothing and enhancement that can be adjusted. Fractional integral-based mask constructions are still not very well understood. Consequently, this study introduces a Caputo fractional integral based mask that maintains isotropic structure while offering customizable nonlocal enhancement characteristics.

III. Methods

A. Construction of the Proposed Mask

One essential method for creating masks is the application of derivative operators and fractional discrete integrals. These operators are distinguished by their special capacity to enlarge the related picture function, which is explained as follows:

$$J^{\alpha}v(t) = \theta_0 v(t) + \theta_1 v(t-1) + \theta_2 v(t-2) + \theta_3 v(t-3) + \ldots \quad (1)$$

where θ_0, θ_1, and θ_2 are the first, second, and third coefficents of the corresponding expansion for the fractional integral or differential definition of J^{α}.

The differential operator corresponding to the fractional calculus with order α with respect to the x-axis and y-axis can be expressed as follows.

$${}^{x}J^{\alpha}v(x,y) = \theta_0 v(x,y) + \theta_1 v(x-1,y) + \theta_2 v(x-2,y) + \ldots \quad (2)$$

$${}^{y}J^{\alpha}v(x,y) = \theta_0 v(x,y) + \theta_1 v(x,y-1) + \theta_2 v(x,y-2) + \ldots \quad (3)$$

We now select a mask with an odd number of dimensions to make sure there is only one central pixel, which is needed for symmetric convolution and proper alignment of the fractional integral weights. This symmetry allows the mask to capture neighborhood information uniformly in all directions, leading to stable enhancement results. By using Eqs. (2) and (3) we consider a fractional integral mask of dimension $(2n+1) \times (2n+1)$ originally developed for image enhancement [19] in the following way.

$$\begin{bmatrix} a_n & \cdots & 0 & 0 & a_n & 0 & 0 & \cdots & a_n \\ \cdots & \cdots & \cdots & \cdots & \cdots & \cdots & \cdots & \cdots & \cdots \\ 0 & \cdots & a_2 & 0 & a_2 & 0 & a_2 & \cdots & 0 \\ 0 & \cdots & 0 & a_1 & a_1 & a_1 & 0 & \cdots & 0 \\ a_n & \cdots & a_2 & a_1 & 8\times a_0 & a_1 & a_2 & \cdots & a_n \\ 0 & \cdots & 0 & a_1 & a_1 & a_1 & 0 & \cdots & 0 \\ 0 & \cdots & a_2 & 0 & a_2 & 0 & a_2 & \cdots & 0 \\ \cdots & \cdots & \cdots & \cdots & \cdots & \cdots & \cdots & \cdots & \cdots \\ a_n & \cdots & 0 & 0 & a_n & 0 & 0 & \cdots & a_n \end{bmatrix}$$

The discrete fractional integral weights are mapped to a spatial convolution mask according to the pixel distance from the center and symmetry considerations. The central coefficient appears as $8a_0$ because the principal fractional weight a_0 contributes along eight symmetric directions surrounding the reference pixel, while pixels at unit and two-pixel distances are assigned a_1 and a_2, respectively. This distance-based allocation ensures rotational symmetry so that the filtering response does not depend on edge orientation. By using the above general mask we can construct a fractional integral mask of dimension 5 × 5 and 7 × 7:

$$\begin{bmatrix} \theta_2 & 0 & \theta_2 & 0 & \theta_2 \\ 0 & \theta_1 & \theta_1 & \theta_1 & 0 \\ \theta_2 & \theta_1 & 8\theta_0 & \theta_1 & \theta_2 \\ 0 & \theta_1 & \theta_1 & \theta_1 & 0 \\ \theta_2 & 0 & \theta_2 & 0 & \theta_2 \end{bmatrix}$$

$$\begin{bmatrix} \theta_3 & 0 & 0 & \theta_3 & 0 & 0 & \theta_3 \\ 0 & \theta_2 & 0 & \theta_2 & 0 & \theta_2 & 0 \\ 0 & 0 & \theta_1 & \theta_1 & \theta_1 & 0 & 0 \\ \theta_3 & \theta_2 & \theta_1 & 8\theta_0 & \theta_1 & \theta_2 & \theta_3 \\ 0 & 0 & \theta_1 & \theta_1 & \theta_1 & 0 & 0 \\ 0 & \theta_2 & 0 & \theta_2 & 0 & \theta_2 & 0 \\ \theta_3 & 0 & 0 & \theta_3 & 0 & 0 & \theta_3 \end{bmatrix}$$

B. *The Mask Using Caputo Fractional Integral*

Out of all the definitions of fractional calculus, the Caputo fractional integral definition is the one employed in this study. The Caputo fractional integral definition is defined as follows:

For a function $f \in L^1[a,b]$, the Caputo fractional integral of order $\alpha > 0$ is defined as Eq. (4).

$${}_{a}^{C}I_{t}^{\alpha} f(t) = \frac{1}{\Gamma(\alpha)} \int_a^t (t-\tau)^{\alpha-1} f(\tau)\, d\tau \quad (4)$$

For numerical computation, we approximate the continuous integral (4) with a discrete sum. To discretize the time domain, we divide the interval [0, t] into n equal subintervals with step size h and time points: $t_0 = 0$, $t_1 = h$, $t_2 = 2h, \ldots, t_n = nh = t$ in order to compute $J^{\alpha}v$ at time t_n. Using a piecewise constant approximation on each subinterval $[t_i, t_{i+1}]$:

$$I^{\alpha}v(t_n) = \frac{1}{\Gamma(\alpha)} \sum_{i=0}^{n-1} \int_{t_i}^{t_{i+1}} (t_n - \tau)^{\alpha-1} v(\tau)\, d\tau \quad (5)$$

Approximating $v(\tau)$ as constant on each subinterval by assuming $v(\tau) \approx v(t_i)$ for $\tau \in [t_i, t_{i+1}]$ and letting $s = t_n - \tau$ in order to evaluate the integral, then:

$$\int_{t_i}^{t_{i+1}} (t_n - \tau)^{\alpha-1} d\tau = \frac{1}{\alpha}\left[\left(t_n - t_i\right)^{\alpha} - \left(t_n - t_{i+1}\right)^{\alpha}\right] \quad (6)$$

Since $t_n - t_i = (n-i)h$ and $t_n - t_{i+1} = (n-i-1)h$:

$$I^{\alpha}v(t_n) = \frac{h^{\alpha}}{\Gamma(\alpha+1)} \sum_{i=0}^{n-1} v(t_i)\left[\left(n-i\right)^{\alpha} - \left(n-i-1\right)^{\alpha}\right] \quad (7)$$

Let $j = n - i - 1$, so when i goes from 0 to $n - 1$, j goes from $n - 1$ to 0:

$$I^{\alpha}v(t_n) = h^{\alpha} \sum_{j=0}^{n-1} \theta_j v(t - jh) \quad (8)$$

where θ_j are the coefficients, computed as Eq. (9):

$$\theta_j = \frac{(j+1)^{\alpha} - j^{\alpha}}{\Gamma(\alpha+1)} \quad (9)$$

For $j = 0, 1, 2,\ldots$, we get $\theta_0 = \frac{1}{\Gamma(\alpha+1)}$, $\theta_1 = \frac{2^\alpha - 1}{\Gamma(\alpha+1)}$, $\theta_2 = \frac{3^\alpha - 2^\alpha}{\Gamma(\alpha+1)}$, $\theta_3 = \frac{4^\alpha - 3^\alpha}{\Gamma(\alpha+1)}$.

Here in this scenario, we consider the 5 × 5 mask and the 7 × 7 mask. The 5 × 5 mask is constructed as below:

$$\begin{bmatrix} \frac{3^\alpha-2^\alpha}{\Gamma(\alpha+1)} & 0 & \frac{3^\alpha-2^\alpha}{\Gamma(\alpha+1)} & 0 & \frac{3^\alpha-2^\alpha}{\Gamma(\alpha+1)} \\ 0 & \frac{2^\alpha-1}{\Gamma(\alpha+1)} & \frac{2^\alpha-1}{\Gamma(\alpha+1)} & \frac{2^\alpha-1}{\Gamma(\alpha+1)} & 0 \\ \frac{3^\alpha-2^\alpha}{\Gamma(\alpha+1)} & \frac{2^\alpha-1}{\Gamma(\alpha+1)} & \frac{8}{\Gamma(\alpha+1)} & \frac{2^\alpha-1}{\Gamma(\alpha+1)} & \frac{3^\alpha-2^\alpha}{\Gamma(\alpha+1)} \\ 0 & \frac{2^\alpha-1}{\Gamma(\alpha+1)} & \frac{2^\alpha-1}{\Gamma(\alpha+1)} & \frac{2^\alpha-1}{\Gamma(\alpha+1)} & 0 \\ \frac{3^\alpha-2^\alpha}{\Gamma(\alpha+1)} & 0 & \frac{3^\alpha-2^\alpha}{\Gamma(\alpha+1)} & 0 & \frac{3^\alpha-2^\alpha}{\Gamma(\alpha+1)} \end{bmatrix}$$

The 7 × 7 mask is constructed as below:

$$\begin{bmatrix} \frac{4^\alpha-3^\alpha}{\Gamma(\alpha+1)} & 0 & 0 & \frac{4^\alpha-3^\alpha}{\Gamma(\alpha+1)} & 0 & 0 & \frac{4^\alpha-3^\alpha}{\Gamma(\alpha+1)} \\ 0 & \frac{3^\alpha-2^\alpha}{\Gamma(\alpha+1)} & 0 & \frac{3^\alpha-2^\alpha}{\Gamma(\alpha+1)} & 0 & \frac{3^\alpha-2^\alpha}{\Gamma(\alpha+1)} & 0 \\ 0 & 0 & \frac{2^\alpha-1}{\Gamma(\alpha+1)} & \frac{2^\alpha-1}{\Gamma(\alpha+1)} & \frac{2^\alpha-1}{\Gamma(\alpha+1)} & 0 & 0 \\ \frac{4^\alpha-3^\alpha}{\Gamma(\alpha+1)} & \frac{3^\alpha-2^\alpha}{\Gamma(\alpha+1)} & \frac{2^\alpha-1}{\Gamma(\alpha+1)} & \frac{8}{\Gamma(\alpha+1)} & \frac{2^\alpha-1}{\Gamma(\alpha+1)} & \frac{3^\alpha-2^\alpha}{\Gamma(\alpha+1)} & \frac{4^\alpha-3^\alpha}{\Gamma(\alpha+1)} \\ 0 & 0 & \frac{2^\alpha-1}{\Gamma(\alpha+1)} & \frac{2^\alpha-1}{\Gamma(\alpha+1)} & \frac{2^\alpha-1}{\Gamma(\alpha+1)} & 0 & 0 \\ 0 & \frac{3^\alpha-2^\alpha}{\Gamma(\alpha+1)} & 0 & \frac{3^\alpha-2^\alpha}{\Gamma(\alpha+1)} & 0 & \frac{3^\alpha-2^\alpha}{\Gamma(\alpha+1)} & 0 \\ \frac{4^\alpha-3^\alpha}{\Gamma(\alpha+1)} & 0 & 0 & \frac{4^\alpha-3^\alpha}{\Gamma(\alpha+1)} & 0 & 0 & \frac{4^\alpha-3^\alpha}{\Gamma(\alpha+1)} \end{bmatrix}$$

C. Evaluation Metrics

In image processing, Mean Square Error (MSE) quantifies the average squared difference between two images, while Peak Signal-to-Noise Ratio (PSNR) measures the ratio of the maximum possible power of a signal to the power of corrupting noise that affects its representation, often used to assess image quality after compression or processing.

The most widely used metric for measuring image quality is Mean Square Error (MSE). This full-reference metric calculates the average square difference between pixels in the original and processed (distorted) image. The processed image is closer to the original image, indicating less distortion or error, when the MSE value is lower. Although MSE offers a numerical representation of the difference between the original and deteriorated images, it is not always correlated with how well an image is perceived by the human eye. According to Miah *et al.* [20] MSE is calculated by averaging the squared intensity differences between the pixels of the original (input) and output images.

$$MSE = \frac{1}{MN}\sum_{i=1}^{M}\sum_{j=1}^{N}\left(I_A\left(i,j\right) - I_B\left(i,j\right)\right)^2 \tag{10}$$

where M and N are the dimensions of the image, $I_A(i, j)$ and $I_B(i, j)$ indicate the original and noisy or denoised images, respectively.

A mathematical indicator of image quality based on the pixel differences between two images is called the signal-to-noise ratio, or SNR. It is frequently used to assess compressed images' quality in comparison to their original. SNR calculates the ratio of a signal's maximum power to the power of corrupting noise that reduces the representation's fidelity. The Mean Squared Error (MSE) of the original and degraded images is used to compute PSNR. It has the following definition and is expressed in decibels (dB):

$$PSNR = 10\log_{10}\left(\frac{MAX^2}{MSE}\right) \tag{11}$$

where MAX is the highest pixel value that can exist (for example, 255 for an 8-bit greyscale image). A better level of fidelity in the compressed image relative to the original image is indicated by higher PSNR values. When evaluating the quality of various compression algorithms or parameter settings, PSNR is especially helpful.

Structural Similarity Index (SSIM) is a widely used metric for evaluating the similarity between two images [29]. It assesses the structural similarity by comparing luminance, contrast, and structure. SSIM provides a measure of similarity between images as a value between −1 and 1, where 1 indicates perfect similarity. So, it considers both luminance and structural similarities.

Firstly, the original and distorted images are divided into blocks of size 8 × 8 and then the blocks are converted into vectors. Secondly, two means two standard deviations, and one covariance value is computed from the images. The mean structural similarity index is computed as follows:

$$SSIM(x,y) = \frac{\left(2\mu_x\mu_y + c_1\right)\left(2\sigma_{xy} + c_2\right)}{\left(\mu_x^2 + \mu_y^2 + c_1\right)\left(\sigma_x^2 + \sigma_y^2 + c_2\right)} \tag{12}$$

This evaluates the similarity between a reference image x and a distorted image y by combining three perceptual components. Mathematically, SSIM is computed using the means μ_x and μ_y, which represent the average intensity of the two images, the variances σ_x^2 and σ_y^2, which measure the contrast or spread of pixel values, and the covariance σ_{xy}, which captures the structural similarity by measuring how the two images vary together. These components are combined into a single formula with small constants c_1 and

c_2 added to ensure numerical stability and avoid division by zero.

IV. Experimental Results

In our work we have used 3 test images: one image of the moon from NASA Earth's Moon, one internet image of a room, and a third image from the Oxford 17 category flower dataset. We applied the 5 × 5 and the 7 × 7 fractional integral mask on each of the images.

A Gaussian noise of $\sigma = 30$ was applied to each of the images and then we recorded the PSNR values for the images at different values of α. Below are the results.

The outcomes of applying a 5 × 5 mask are shown in Figs. 1–3, whereas the results of applying a 7 × 7 mask are shown in Figs. 4–6.

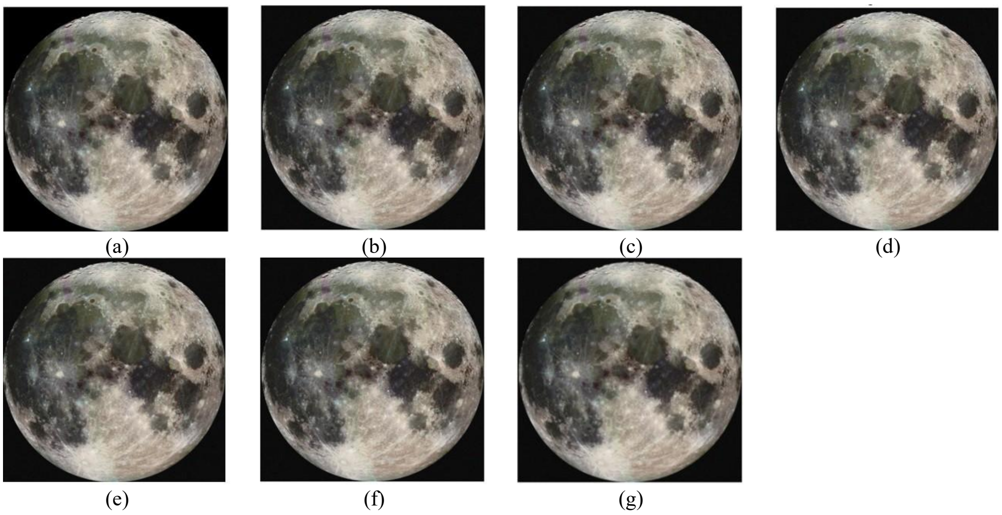

Fig. 1. Enhancement results for the moon image using the proposed 5 × 5 fractional integral mask: (a) Original image, (b) Noisy Image, (c) $\alpha = 0.2$, (d) $\alpha = 0.4$, (e) $\alpha = 0.8$, (f) $\alpha = 0.99$, (g) $\alpha = 0.9999$.

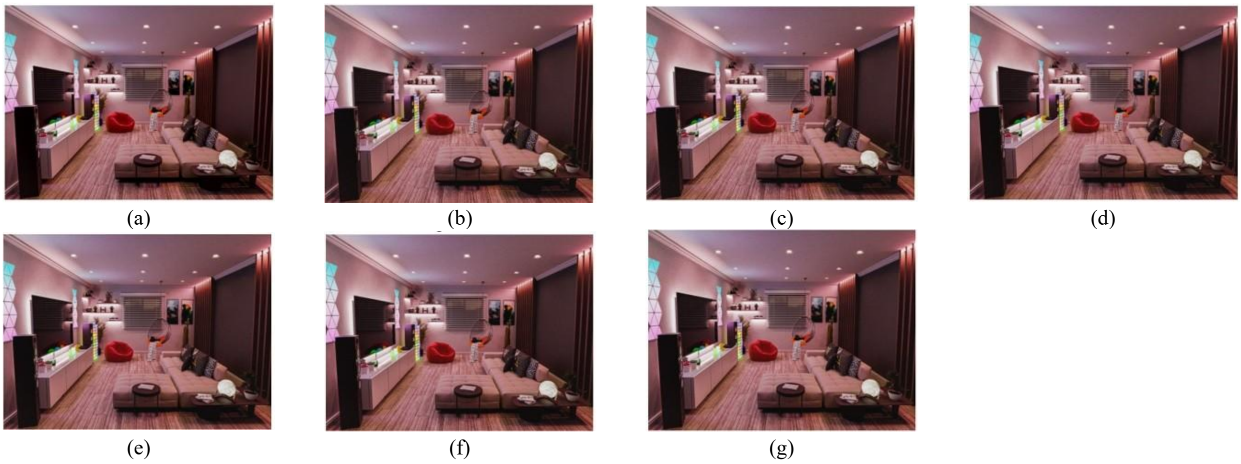

Fig. 2. Enhancement results for the room image using the proposed 5 × 5 fractional integral mask: (a) Original image, (b) Noisy Image, (c) $\alpha = 0.2$, (d) $\alpha = 0.4$, (e) $\alpha = 0.8$, (f) $\alpha = 0.99$, (g) $\alpha = 0.9999$.

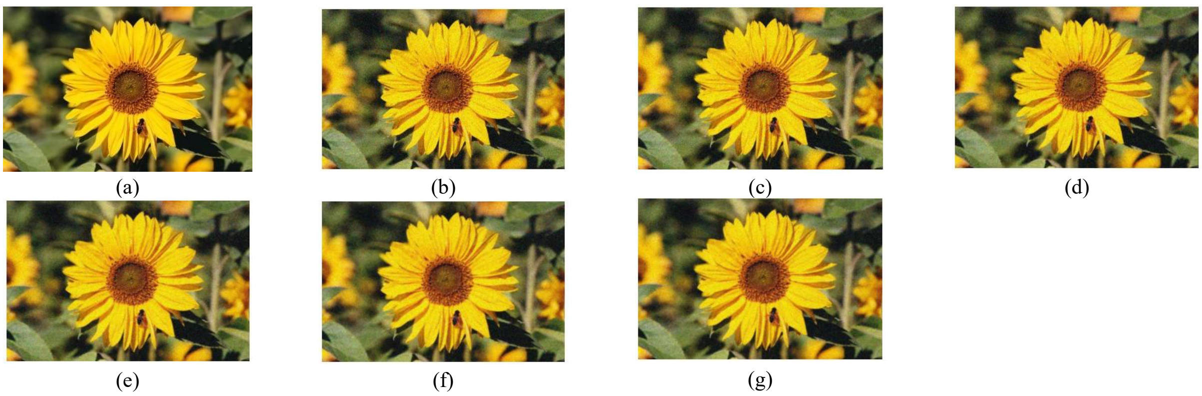

Fig. 3. Enhancement results for the flower image using the proposed 5 × 5 fractional integral mask: (a) Original image, (b) Noisy Image, (c) $\alpha = 0.2$, (d) $\alpha = 0.4$, (e) $\alpha = 0.8$, (f) $\alpha = 0.99$, (g) $\alpha = 0.9999$.

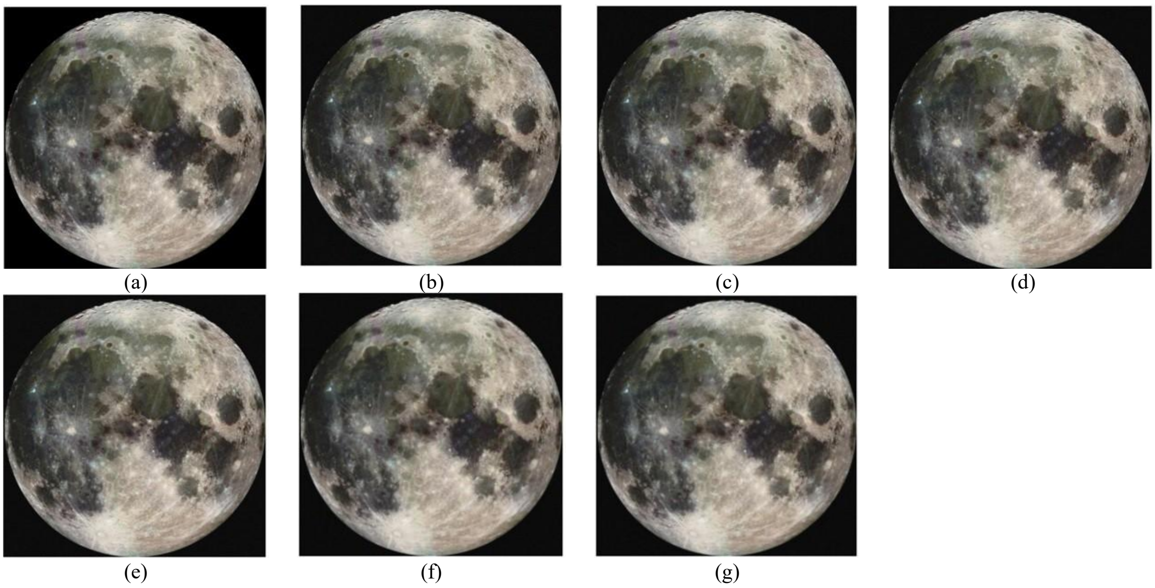

Fig. 4. Enhancement results for the moon image using the proposed 7 × 7 fractional integral mask: (a) Original image, (b) Noisy Image, (c) $\alpha = 0.2$, (d) $\alpha = 0.4$, (e) $\alpha = 0.8$, (f) $\alpha = 0.99$, (g) $\alpha = 0.9999$.

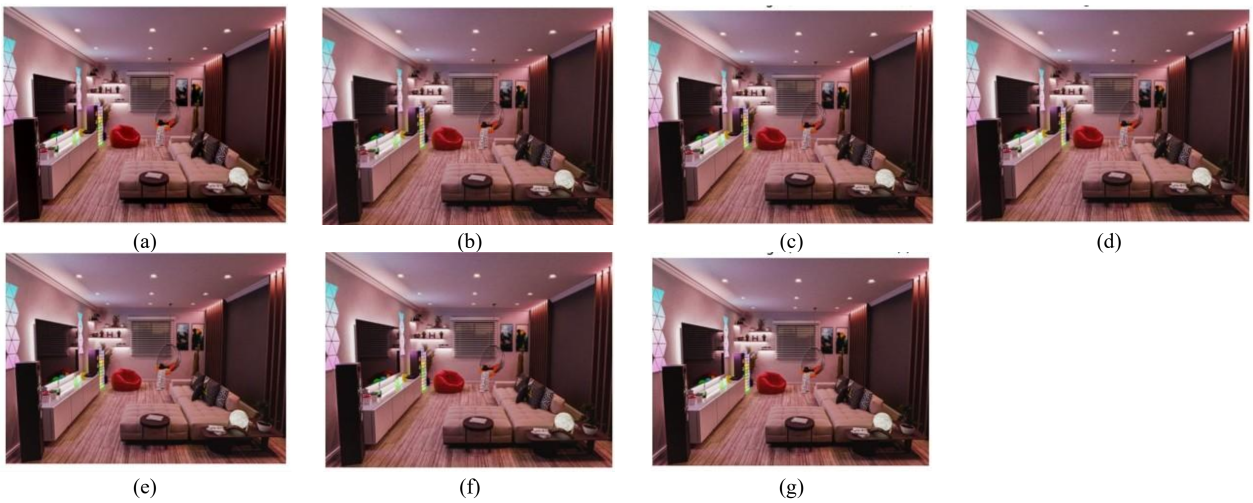

Fig. 5. Enhancement results for the room image using the proposed 7 × 7 fractional integral mask: (a) Original image, (b) Noisy Image, (c) $\alpha = 0.2$, (d) $\alpha = 0.4$, (e) $\alpha = 0.8$, (f) $\alpha = 0.99$, (g) $\alpha = 0.9999$.

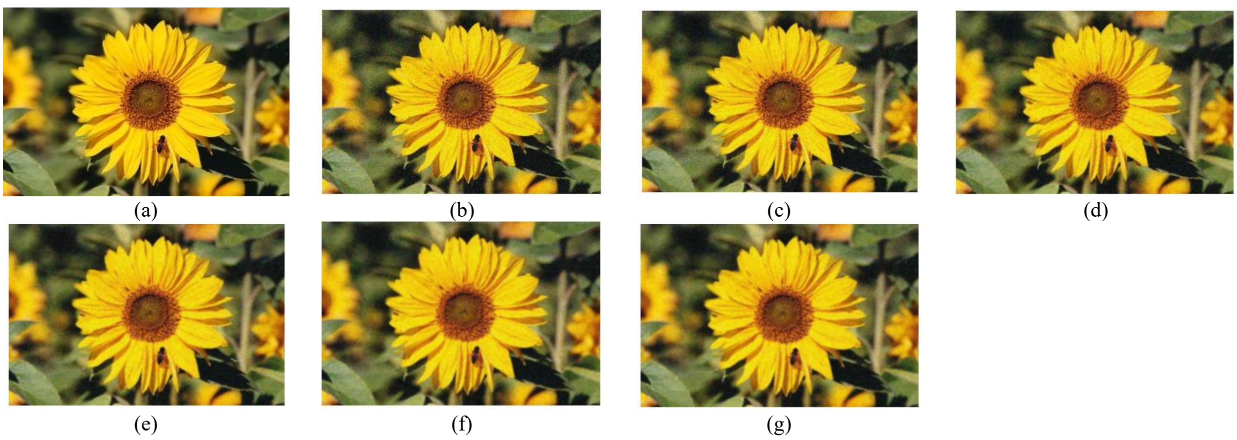

Fig. 6. Enhancement results for the flower image using the proposed 7 × 7 fractional integral mask: (a) Original image, (b) Noisy Image, (c) $\alpha = 0.2$, (d) $\alpha = 0.4$, (e) $\alpha = 0.8$, (f) $\alpha = 0.99$, (g) $\alpha = 0.9999$.

The following observations were drawn from the experiment that was performed on the three images.

(1) Applying a 5 × 5 mask to the moon image produced a higher quality image with a PSNR value of 26.15 with fractional-order $\alpha = 0.9999$ and

$\sigma = 30$, while using a 7×7 mask produced a higher quality image with a PSNR value of 26.68 with fractional-order $\alpha = 0.9999$ and $\sigma = 30$.

(2) Applying a 5×5 mask to the room image resulted in an improved quality image with $\alpha = 0.9999$ and PSNR value = 25.90 and σ =30. Similarly, applying a 7×7 mask to the same image produced an improved quality image with $\alpha = 0.9999$, $\sigma = 30$ and PSNR = 26.27.

(3) Applying a 5×5 mask to the flower image resulted in a higher quality image with $\alpha = 0.9999$, $\sigma = 30$ and PSNR = 26.53. Applying a 7×7 mask to the same image produced a PSNR = 27.32 with $\alpha = 0.9999$, $\sigma = 30$.

From the results above, we can infer that the image's visual quality improved as the PSNR value rose as the fractional-order got closer to 1. Additionally, compared to a 5×5, a 7×7 mask produced better results.

Table I presents the PSNR (in dB) values and Table II presents the SSIM values corresponding to the moon, room, and flower images, respectively, for varying values of the fractional-order α using 5×5 and 7×7 masks.

TABLE I. COMPARATIVE STUDY OF FILTERS IN TERMS OF PSNR FOR DIFFERENT IMAGES

α	Moon 5 × 5	Moon 7 × 7	Room 5 × 5	Room 7 × 7	Flower 5 × 5	Flower 7 × 7
0.1	20.12	20.34	20.08	20.31	20.31	20.53
0.2	20.98	21.42	20.96	21.39	21.20	21.64
0.3	21.81	22.37	21.81	22.42	22.06	22.69
0.4	22.60	23.34	22.61	23.33	22.86	23.68
0.5	23.36	24.15	23.35	24.16	23.65	24.54
0.6	24.03	24.87	24.06	24.85	24.36	25.36
0.7	24.66	25.64	24.62	25.40	25.03	26.03
0.8	25.30	25.86	25.13	25.79	25.58	26.57
0.9	25.74	26.46	25.56	26.12	26.13	26.97
0.99	26.00	26.64	25.88	26.24	26.26	27.27
0.9999	26.15	26.68	25.90	26.27	26.53	27.32

TABLE II. COMPARATIVE STUDY OF FILTERS IN TERMS OF SSIM FOR DIFFERENT IMAGES

α	Moon 5 × 5	Moon 7 × 7	Room 5 × 5	Room 7 × 7	Flower 5 × 5	Flower 7 × 7
0.1	0.469	0.573	0.507	0.637	0.334	0.347
0.2	0.801	0.873	0.728	0.761	0.620	0.654
0.3	0.799	0.626	0.729	0.616	0.340	0.380
0.4	0.610	0.535	0.508	0.713	0.795	0.730
0.5	0.768	0.911	0.617	0.614	0.378	0.337
0.6	0.760	0.525	0.631	0.483	0.378	0.365
0.7	0.729	0.611	0.577	0.513	0.389	0.421
0.8	0.473	0.579	0.919	0.368	0.759	0.691
0.9	0.574	0.746	0.564	0.602	0.331	0.384
0.99	0.682	0.816	0.819	0.473	0.818	0.533
0.9999	0.958	0.602	0.597	0.595	0.717	0.705

The generated SSIM values range from 0.331 to 0.958, indicating that the performance of the Caputo fractional integral approach is highly dependent on the fractional order α and the picture properties. For the 5×5 mask, applied on Moon image at $\alpha = 0.9999$ (SSIM = 0.958) and Room image at $\alpha = 0.8$ (SSIM = 0.919), the proposed technique achieves excellent structural similarity indicating that it retains structural information better. The 5×5 kernel consistently outperforms the other kernels on all kinds of images. This implies that structural properties are better preserved by smaller kernels. The type of image determines the optimal fractional orders, where the Moon images perform best overall. These findings demonstrate that the Caputo fractional technique produces objective pixel-level gains while maintaining a high perceptual quality.

The enhancement behavior can be explained by the discretized Caputo fractional weights θ_i, which control the contribution of neighboring pixels. For small α, the weights decay slowly, resulting in strong nonlocal averaging and image blurring. As α increases, the weights become more localized, reducing smoothing and preserving edges. In the limit $\alpha \to 1$, the operator approaches the classical integral, explaining the improved PSNR and SSIM values observed experimentally.

In Figs. 7–9, the PSNR values for both masks are plotted against the fractional-order α or the moon, room, and flower images. In all three cases, the 7×7 mask demonstrates slightly higher PSNR values compared to the 5×5 mask, indicating its superior performance in image enhancement, particularly at higher fractional-orders. Larger masks appear to be more effective in reducing noise and improving image quality, especially in the context of fractional calculus-based filtering.

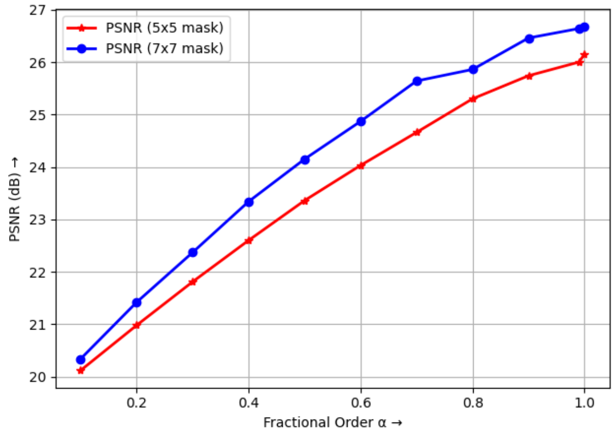

Fig. 7. Variation of PSNR with respect to the fractional-order α for the Moon image evaluated using the 5×5 and 7×7 enhancement masks.

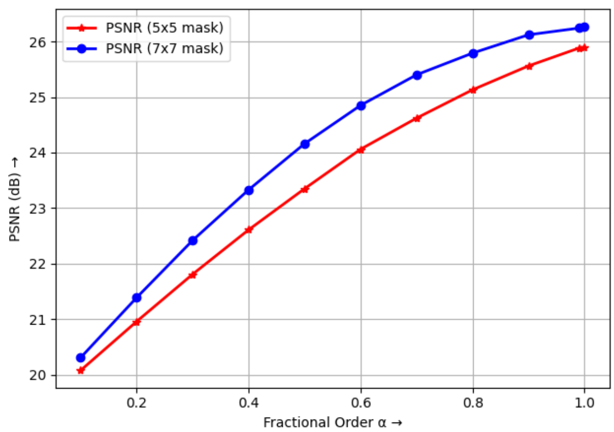

Fig. 8. Variation of PSNR with respect to the fractional-order α for the Room image evaluated using the 5×5 and 7×7 enhancement masks.

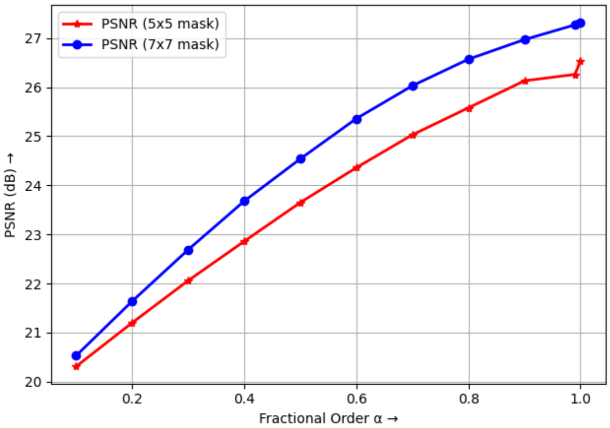

Fig. 9. Variation of PSNR with respect to the fractional-order α for the Flower image evaluated using the 5 × 5 and 7 × 7 enhancement masks.

V. Conclusion

Our study demonstrates the potential of fractional calculus as a flexible and effective framework for image enhancement. By adapting the mask structure to the Caputo based weights, this approach enables selective enhancement of weak edges and textures while concurrently minimizing Gaussian noise. Using a fractional order between 0 and 1, we apply 5 × 5 and 7 × 7 fractional integral masks to various images. For small α, the operator behaves as a strong averaging filter, leading to blurring, whereas values of α close to 1 yield sharper structures and higher PSNR, leading to close resemblance to the original images.

The Caputo fractional integral method demonstrates excellent perceptual quality with SSIM values exceeding 0.90 for optimal parameter configurations α = 0.5–0.9999 with 5 × 5 kernel, confirming dual verification through both objective pixel-level metrics and structural similarity preservation across diverse image types.

The presented framework has practical value for applications such as low contrast imaging and texture rich scenes. Future work will include additional evaluation metrics, broader image datasets, and comparisons with other enhancement techniques.

Conflict of Interest

The authors declare no conflict of interest.

Author Contributions

Varsha S N contributed to conceptualization, methodology, data curation, investigation, formal analysis, implementation, writing of the original draft, and performed the Python experiments. Sowmya M supervised the study, participated in the research design and results validation, and assisted in the review and editing of the manuscript. All authors have read and approved the final version of the manuscript.

References

[1] K. B. Oldham and J. Spanier, *The Fractional Calculus: Theory and Applications of Differentiation and Integration to Arbitrary Order*. New York: Academic Press, 1974.

[2] R. C. Gonzalez and R. E. Woods, *Digital Image Processing*, 4th ed. London, UK: Pearson, 2018.

[3] T. Acharya and A. K. Ray, *Image Processing: Principles and Applications*. Hoboken, NJ, USA: Wiley, 2005.

[4] Y. Zhang, Y. Pu, and J. Zhou, "Construction of fractional differential masks based on Riemann–Liouville definition," *J. Comput. Inf. Syst.*, vol. 6, pp. 3191–3199, 2010.

[5] X. Chen and X. Fei, "Improving edge-detection algorithm based on fractional differential approach," in *Proc. Int. Conf. Image, Vis. Comput.*, Singapore, 2012, vol. 50.

[6] V. Garg and K. Singh, "An improved Grünwald–Letnikov fractional differential mask for image texture enhancement," *International Journal of Advanced Computer Science and Applications*, vol. 3, no. 3, pp. 130–135, 2012.

[7] Q. Yu, F. Liu, I. Turner, K. Burrage, and V. Vegh, "The use of a Riesz fractional differential-based approach for texture enhancement in image processing," *ANZIAM Journal*, vol. 54, pp. 590–607, 2013.

[8] S. S. Bedi and R. Khandelwal, "Various image enhancement techniques-A critical review," *International Journal of Advanced Research in Computer and Communication Engineering,* vol. 2, no. 3, pp. 1605–1609, 2013.

[9] M. Caputo and M. Fabrizio, "A new definition of fractional derivative without singular kernel," *Progress in Fractional Differentiation and Applications*, vol. 1, no. 2, pp. 73–85, 2015.

[10] P. Amoako-Yirenkyi, J. K. Appati, and I. K. Dontwi, "A new construction of a fractional derivative mask for image edge analysis based on Riemann-Liouville fractional derivative," *Advances in Difference Equations*, vol. 2016, no. 1, 238, 2016.

[11] P. Amoako-Yirenkyi, J. K. Appati, and I. K. Dontwi, "Performance analysis of image smoothing techniques on a new fractional convolution mask for image edge detection," *Open Journal of Applied Sciences*, vol. 6, no. 7, pp. 478–488, 2016.

[12] M. V. Kumar and P. Suresh, "Detection and segmentation of lung cancer on CT images by using fractional calculus," *JETIR*, vol. 5, no. 5, pp. 520–525, 2018.

[13] W. S. Araby, A. H. Madian, M. A. Ashour, I. Farag, and M. Nassef, "Radiographic images fractional edge detection based on genetic algorithm," *WSEAS Transactions on Information Science and Applications*, vol. 15, pp. 168–176, 2018.

[14] H. Ackar, A. A. Almisreb, and M. A. Saleh, "A review on image enhancement techniques," *Southeast Europe Journal of Soft Computing*, vol. 8, no. 1, pp. 42–48, 2019.

[15] J. E. Lavín-Delgado, J. E. Solís-Pérez, J. F. Gómez-Aguilar, and R. F. Escobar-Jiménez, "A new fractional-order mask for image edge detection based on Caputo-Fabrizio fractional-order derivative without singular kernel," *Circuits, Systems, and Signal Processing*, vol. 39, no. 3, pp. 1419–1448, 2020.

[16] N. Aboutabit, "A new construction of an image edge detection mask based on Caputo–Fabrizio fractional derivative," *The Visual Computer*, vol. 37, no. 6, pp. 1545–1557, 2021.

[17] B. Ghanbari and A. Atangana, "Some new edge detecting techniques based on fractional derivatives with non-local and non-singular kernels," *Advances in Difference Equations*, vol. 2020, no. 1, 435, 2020.

[18] X. Lin, Y. Wang, G. Wu, and J. Hao, "Image denoising of adaptive fractional operator based on Atangana–Baleanu derivatives," *Journal of Mathematics*, vol. 2021, no. 1, 5581944, 2021.

[19] R. Tang and B. Liu, "Application of fractional differential model in image enhancement of strong reflection surface," *Mathematics*, vol. 11, no. 2, 444, 2023.

[20] B. A. Miah, M. Sen, R. Murugan, and D. Gupta, "Developing Riemann–Liouville-fractional masks for image enhancement," *Circuits, Systems and Signal Processing*, vol. 43, no. 6, pp. 3802–3831, 2024.

[21] M. Henriques, D. Valério, P. Gordo, and R. Melicio, "Fractional-order colour image processing," *Mathematics*, vol. 9, no. 5, 457, 2021.

[22] G. A. M. Nchama, A. L. Meclais, L. D. L. Alfonso, and M. R. Ricard, "Construction of Caputo-Fabrizio fractional differential

mask for image enhancement," *Progress in Fractional Differentiation and Applications*, vol. 7, no. 2, pp. 87–96, 2021.

[23] A. R. Al-Shamasneh and R. W. Ibrahim, "Image denoising based on quantum calculus of local fractional entropy," *Symmetry*, vol. 15, no. 2, 396, 2023.

[24] Y. Yu and C. Qin, "An end-to-end underwater-image-enhancement framework based on fractional integral retinex and unsupervised autoencoder," *Fractal and Fractional*, vol. 7, no. 1, 70, 2023.

[25] A. Nosheen, M. Tariq, K. A. Khan, N. A. Shah, and J. D. Chung, "On Caputo fractional derivatives and Caputo–Fabrizio integral operators via (s, m)-convex functions," *Fractal and Fractional*, vol. 7, no. 2, 2023.

[26] M. Medveď, M. Pospíšil, and E. Brestovanská, "Nonlinear integral inequalities involving tempered Ψ-Hilfer fractional integral and fractional equations with tempered Ψ-Caputo fractional derivative," *Fractal and Fractional*, vol. 7, no. 8, 2023.

[27] I. T. Huseynov, A. Ahmadova, and N. I. Mahmudov, "Fractional Leibniz integral rules for Riemann–Liouville and Caputo fractional derivatives and their applications," arXiv Preprint, arXiv:2012.11360, 2020.

[28] Y. F. Pu, J. L. Zhou, and X. Yuan, "Fractional differential mask: A fractional differential-based approach for multiscale texture enhancement," *IEEE Trans. on Image Processing*, vol. 19, no. 2, pp. 491–511, 2010.

[29] Y. Al Najjar, "Comparative Analysis of Image Quality Assessment Metrics: MSE, PSNR, SSIM and FSIM," *International Journal of Science and Research*, vol. 13, no. 3, 2024.